

Observation of a dissipative time crystal in a strongly interacting Rydberg gas

Xiaoling Wu,^{1,*} Zhuqing Wang,^{1,*} Fan Yang,^{2,*} Ruochen Gao,¹ Chao Liang,¹
Meng Khoon Tey,^{1,3,4} Xiangliang Li,^{5,†} Thomas Pohl,^{2,‡} and Li You^{1,3,4,5,§}

¹*State Key Laboratory of Low Dimensional Quantum Physics,
Department of Physics, Tsinghua University, Beijing 100084, China*

²*Center for Complex Quantum Systems, Department of Physics and Astronomy,
Aarhus University, DK-8000 Aarhus C, Denmark*

³*Frontier Science Center for Quantum Information, Beijing 100084, China*

⁴*Hefei National Laboratory, Hefei, Anhui 230088, China*

⁵*Beijing Academy of Quantum Information Sciences, Beijing 100193, China*

The notion of spontaneous symmetry breaking has been well established to characterize classical and quantum phase transitions of matters, such as in condensation, crystallization, and quantum magnetism, etc. Generalizations of this paradigm to the time dimension can further lead to an exotic dynamical phase, the time crystal, which spontaneously breaks the time translation symmetry of the system [1]. While the existence of a continuous time crystal at equilibrium has been challenged by the no-go theorems [2, 3], the difficulty can be circumvented by the dissipation in an open system. Here, we report the experimental observation of such a dissipative time crystalline order in a room-temperature atomic gas, where ground-state atoms are continuously driven to Rydberg states via electromagnetically induced transparency (EIT). The emergent time crystal is revealed by persistent oscillations of the probe-field transmission, with ultralong lifetime and no observable damping during the measurement. We show that the observed limit cycles arise from the coexistence and competition between distinct Rydberg components, in agreement with a mean-field analysis derived from the microscopic model. The random phase distribution of the oscillation for repeated realizations, together with the robustness against temporal noises further supports our realization of a dissipative time crystal.

The search for emergent many-body phases is among the central objectives of quantum physics [4]. While the concept of phase transitions in thermal equilibrium is well developed, the presence of driving and dissipation can result in a rich phenomenology that has no counterpart in equilibrium [5], such as ubiquitous self-organization effects in physics, biology, and economics [6]. In particular, such nonequilibrium processes can facilitate a novel dynamical phase that spontaneously breaks time translation symmetry, commonly referred to as a time crystal [7–31]. In analogy to crystals in space, a continuous time crystal (CTC) phase has an order parameter with self-sustained oscillations, even though the system is driven in a continuous manner. A dissipative CTC has been recently observed with atomic Bose-Einstein condensate in an optical cavity [32]. The inevitable loss of atoms in the ultracold regime, however, complicates the investigation of long-time dynamics and thereby hinders the analysis of long-range time crystalline order.

Ensembles of Rydberg atoms represent a suitable platform for exploring many-body phenomena away from equilibrium emerging from coherent driving, dissipation, and long-range dipole-dipole interactions [33–39]. Such a Rydberg gas is well controllable and can be confined in a room-temperature vapour cell at virtually no atom

loss. Here, we exploit this feature and report the experimental observation of long-range time crystalline order in a continuously driven Rydberg gas [see Fig. 1(a)]. In our experiment, the CTC manifests itself in limit cycle oscillations of the Rydberg atom density and the atomic dipole moment, which we probe directly by the transmission of light through the gas [see Fig. 1(b)]. We demonstrate that the time crystal originates from the competition between atomic excitations in different Rydberg states, and characterize the parameter regimes that support this phase. We verify the observation of a CTC by experimentally demonstrating the continuous nature of the symmetry breaking and its robustness against noisy temporal perturbations.

To understand the origin of the limit cycle in our experiment, we first consider the microscopic description of the driven-dissipative Rydberg gas. As illustrated in Fig. 1(c), the applied laser fields generated a coherent coupling between the atomic ground state $|g\rangle$ and a Rydberg state $|r\rangle$, with a corresponding Rabi frequency Ω and frequency detuning Δ , while spontaneous decay leads to a loss of coherence and Rydberg population with a rate γ . The strong interaction between Rydberg states is governed by a Hamiltonian $\hat{H}_1 = \sum_{i \neq j} (V_{ij}/2) \hat{n}_i \hat{n}_j$, with $\hat{n}_i = |r_i\rangle \langle r_i|$ the local Rydberg density and $V_{ij} = C_6/|\mathbf{r}_i - \mathbf{r}_j|^6$ the van der Waals interaction between Rydberg atoms located at \mathbf{r}_i and \mathbf{r}_j . In a thermal Rydberg gas, however, the atomic motion averages out the associated spatial correlations between Rydberg atoms and permits a mean-field treatment of the interaction [35], whereby the laser detuning $\Delta \rightarrow \Delta - \chi n_r$ acquires a

* These authors contributed equally to this work

† lixl@baqis.ac.cn

‡ pohl@phys.au.dk

§ lyou@mail.tsinghua.edu.cn

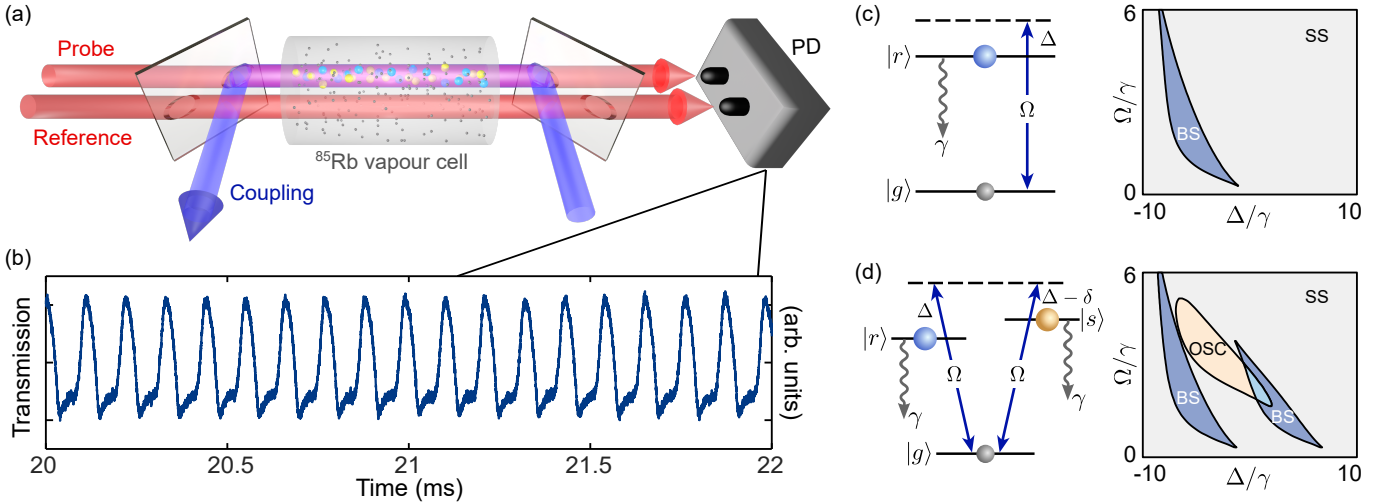


FIG. 1. (a) Schematic of the experimental setup, where a probe and an identical reference beam are propagating in parallel through a room-temperature ^{85}Rb vapour cell, with the probe beam overlapping with a counterpropagating coupling beam. The transmission signals of the probe and the reference beams are detected by a balanced photon detector (PD) for differential measurement. The waist of the probe (coupling) beam is around $500\ \mu\text{m}$, which yields a maximum Rabi frequency $\sim 2\pi \times 40\ \text{MHz}$ ($\sim 2\pi \times 2\ \text{MHz}$) in our experiment. (b) Measured transmission signals for the principal quantum number $n = 75$. (c) The left and the right panel respectively show the level scheme and the mean-field phase diagram for the case of a single Rydberg state $|r\rangle$ with $\chi = -16\gamma$, which supports a stationary phase (SS) and a bistable phase (BS). (d) The left and the right panel respectively show the level scheme and the phase diagram for a system involving two Rydberg states $|r\rangle$ and $|s\rangle$ with $\chi = -16\gamma$ and $\delta = 8\gamma$. Here, a limit cycle oscillating phase (OSC) is identified. The overlapping region between an OSC phase and a BS phase contains one stationary state and one stable limit cycle.

dependence on the uniform Rydberg density $n_r = \langle \hat{n}_r \rangle$, with an effective nonlinearity strength χ . The finite decay rate γ usually relaxes the system to a stationary mixed state (SS), corresponding to the fixed point of the nonlinear optical Bloch equation. However, it has been shown that the interaction induced nonlinearity can cause a saddle-node bifurcation [35], through which a bistable stationary state emerges in a finite region of the parameter space. For an attractive interaction ($\chi < 0$), such a bistable phase (BS) can occur at the negative detuning regime [see the right panel of Fig. 1(c)]. At its boundaries one finds a discontinuous nonequilibrium transition between distinct stationary states with low and high Rydberg-state concentration, respectively.

The situation changes dramatically when more than one Rydberg states come into play. In order to illustrate this effect, we consider a minimal extension, in which one additional Rydberg state $|s\rangle$ is coupled with an identical Rabi frequency Ω but different detuning $\Delta - \delta$, [see Fig. 1(d)]. These distinct Rydberg states can establish their respective bistable phases at different detunings Δ for a sufficiently large energy separation δ . More importantly, their strong interactions generate nonlinearities, $\chi(n_r + n_s)$, that couple the dynamics of both Rydberg states. The resulting competition can drive a Hopf bifurcation for $\chi \sim \delta$, whereby a non-stationary dynamical phase appears in between the two bistable regions, as illustrated in the right panel of Fig. 1(d). In this non-stationary regime, the interaction can facilitate the ex-

citation of one Rydberg state at the cost of the other, leading to limit cycle dynamics with persistent oscillations of the Rydberg densities without damping.

The experimental setup for observing such an oscillatory dynamics is depicted in Fig. 1(a), where ^{85}Rb atoms of an average spacing $\sim 2.4\ \mu\text{m}$ are trapped in a 7.5-cm-long room-temperature vapour cell. The atoms are continuously excited to the Rydberg states via a two-photon process, in which a 780-nm probe beam and a 480-nm coupling beam counterpropagates with each other. Here, the probe and the coupling fields drive the ground state manifold $|5S_{1/2}, F = 3\rangle$ to the Rydberg manifold $|nD_J\rangle$ ($J = 5/2, 3/2$) via intermediate states $|5P_{3/2}, F = 4\rangle$. The exact Zeeman level of the states can be specified by the polarization of the beams [see Fig. 2(a)]. In the limit cycle phase, the dynamics imposes an oscillation of the transition dipoles between these states, which results in an oscillating transmission of the probe field. To obtain a clear EIT signal, we use a calcite beam displacer to generate a reference beam parallel to the probe beam for differential measurement. The transmission signal for a high lying Rydberg state $n = 75$ is shown in Fig. 1(b), which exhibits a stable periodic oscillation pattern. In this single experiment, six Rydberg states close in energy are involved in the driving scheme [40], and should all participate in the synchronized oscillating dynamics.

To confirm that the oscillation is indeed induced by the involvement of multiple Rydberg states, we reduce the principal quantum number of the Rydberg states to

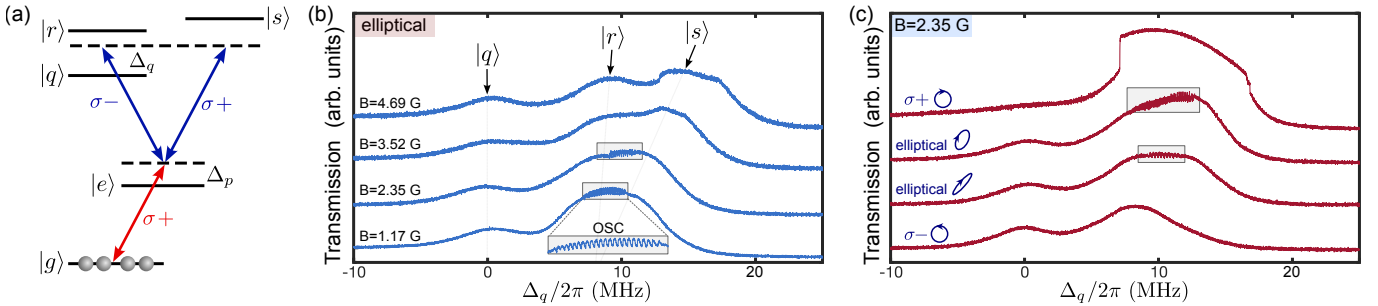


FIG. 2. (a) EIT level diagram for the Rydberg excitation scheme. The ground state $|g\rangle = |5S_{1/2}, F = 3, m_F = 3\rangle$ is coupled to an intermediate state $|e\rangle = |5P_{3/2}, F = 4, m_F = 4\rangle$ by a $\sigma+$ polarized 780-nm probe field, and three Rydberg Zeeman sublevels $|r\rangle = |nD_{5/2}, m_J = 1/2\rangle$, $|s\rangle = |nD_{5/2}, m_J = 5/2\rangle$, $|q\rangle = |nD_{3/2}, m_J = 1/2\rangle$ are further connected by a 480-nm coupling field. (b) Scanned transmission spectrum for the different indicated magnetic fields at elliptical polarized coupling field. (c) Scanned transmission spectrum for the different indicated polarizations at low magnetic field $B = 2.35$ G. The principle quantum number here is $n = 69$ and the scanning rate is $2\pi \times 0.67$ MHz/ms.

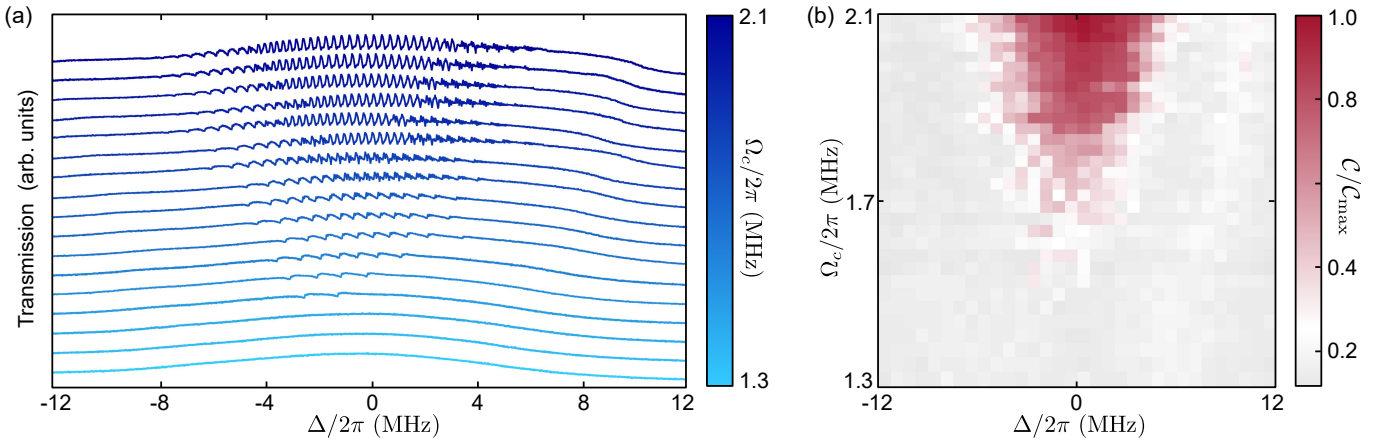


FIG. 3. Mapping of the crystalline regime. (a) Evolution of the scanned transmission spectrum at increasing Rabi frequency Ω_c from down to up with $\Omega_p/2\pi = 40$ MHz and $\Delta_p/2\pi = 100$ MHz. The scanning rate is $2\pi \times 2$ MHz/ms, and the curves are offset vertically for clarity. (b) Extracted phase diagram for the oscillation contrast ratio.

$n = 69$ and apply a magnetic field B to adjust the energy differences between distinct Zeeman levels. Then, with a careful choice of the polarization, we can study the dynamics mainly involving two Rydberg states close in energy, i.e., states $|r\rangle$ and $|s\rangle$ in Fig. 2(a). The branching ratio of the coupling to these states can be tuned by the polarization of the coupling field [40]. In order to identify the region displaying limit cycles, we perform a scanning EIT spectroscopy measurement, in which the frequency of the coupling beam is slowly scanned near the two-photon resonance with a fixed intermediate-state detuning Δ_p . In the scanning process, the magnetic insensitive Rydberg level $|q\rangle = |69D_{3/2}, m_J = 1/2\rangle$ separated from the two target states can also be laser coupled, and is chosen as a reference state with a detuning Δ_q .

The observed EIT spectrum for different magnetic fields and polarizations are shown in Figs. 2(b) and 2(c). First, we set the polarization of coupling beam to be elliptical, by which both Rydberg states can be excited, and they are distinguishable at a large magnetic field $B = 4.69$ G [see Fig. 2 (b)]. Crucially, oscillations ap-

pear only in the case of a relatively small magnetic field, where $|r\rangle$ and $|s\rangle$ are close enough to induce the competition. Next, we fix the magnetic field at a small value $B = 2.35$ G and vary the polarization of the coupling light [see Fig. 2(c)]. We find the oscillating phase only exists at an elliptical polarization, but disappears for a perfectly circularly polarized case σ_- or σ_+ , where only one of the Rydberg states $|r\rangle$ or $|s\rangle$ is excited. Based on the experimental evidences above, we conclude that it is the competition between multiple Rydberg levels facilitating the limit cycle phase, in agreement with the mean-field prediction.

In addition to multiple Rydberg components, sufficiently large Rabi frequencies of the probe (Ω_p) and the coupling (Ω_c) are also necessary to induce the limit cycle. Figure 3(a) displays the scanning EIT spectrum at different Ω_c with a large and fixed Ω_p , from which rich oscillating patterns can be identified. First, we note that the oscillation completely disappears if the Rabi frequency is too small. Then, weak and long-period oscillations come into appearance when Ω_c slightly exceeds a certain

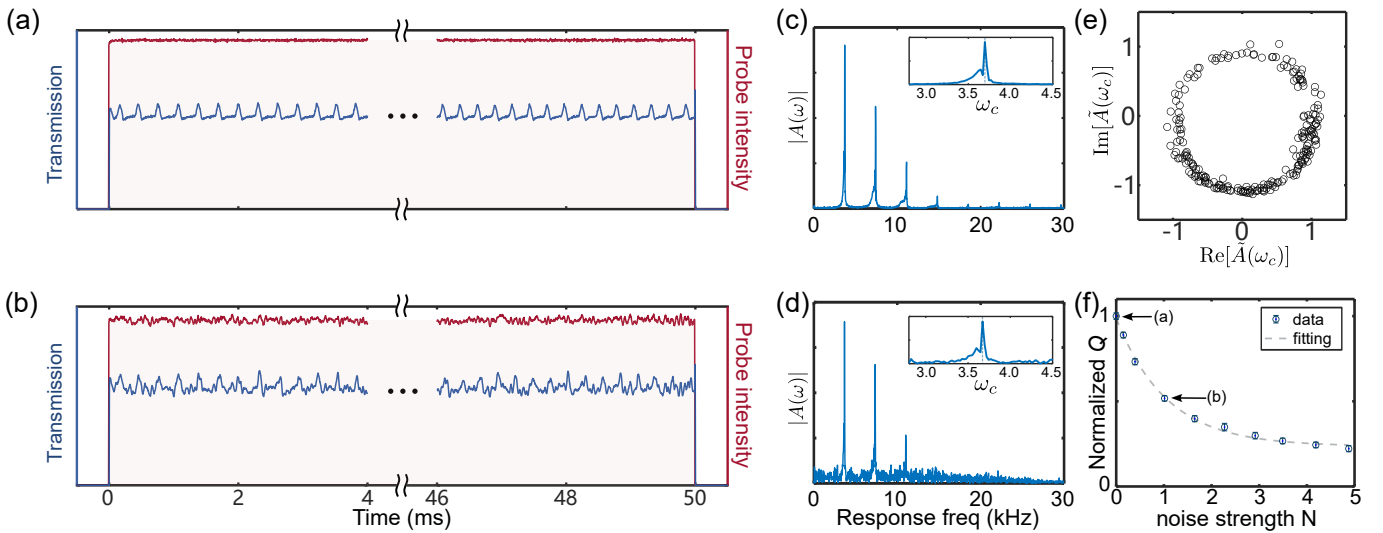


FIG. 4. Breaking of continuous time translation symmetry and the robustness against temporal perturbations. (a) and (b) respectively show a single realization of sustained oscillation transmission (dark blue) with and without intensity noise on probe laser field. The red lines represent the probe intensity monitored by an independent PD. (c) and (d) are discrete Fourier transform power spectrum of (a) and (b). (e) Distribution of the time phase of the time oscillation. (f) Relative crystalline fraction for varying noise strength at parameters $\{\Delta_p, \Omega_p, \Omega_c\}/2\pi = \{100, 34, 2\}$ MHz. The noise strength is defined as $N = \sum_{\omega \in \Delta\omega} |A_n(\omega)| / \sum_{\omega \in \Delta\omega} |A_{n-\text{free}}(\omega)| - 1$, where $|A_n(\omega)|$ and $|A_{n-\text{free}}(\omega)|$ correspond to the power spectra with and without noise, respectively. The decay of the crystalline fraction is fitted as $Q/Q_{\max} = 0.75 \times \exp(-0.94N) + 0.25$.

critical point. As Rabi frequency is further increased, the amplitude of the oscillation as well as its range increases. Interestingly, some small-amplitude oscillations of short periods ($\sim 30 \mu\text{s}$) embedded in long-period ones ($\sim 150 \mu\text{s}$) are observed. The patterns of oscillations become even richer at a larger Ω_c , and the system seems to exhibit unstable chaotic behaviors near the phase boundary. Choosing the oscillating contrast ratio \mathcal{C} as the order parameter, we can extract an approximate phase diagram from the scanning EIT spectrum, as shown in Fig. 3 (b), where limit cycle phase is revealed by a nonvanishing contrast. Concerning the finite scanning rate, the phase boundary can be approximately determined by a cut-off value $\mathcal{C} = 0.2\mathcal{C}_{\max}$. The measured phase diagram indicates that the limit cycle phase exists over a wide parameter regimes and is not sensitive to experimental conditions, such as laser power and frequency, etc.

Having explored the parameter regions supporting the limit cycle, we now focus on the oscillating behavior at fixed parameters, corresponding to a time translation invariant system. Specifically, we investigate a quench dynamics, where the probe field is suddenly turned on by an acoustic optical modulator (AOM) and then held at a constant strength for a very long time. As shown in Fig. 4(a), an oscillation pattern is established in a relaxation time $\sim 200 \mu\text{s}$, and then sustains in the entire continuous driving window of 50 ms. This persistent oscillation is a clear evidence of the time translation symmetry breaking, and thus indicates a possible time crystalline order. A discrete Fourier transform (DFT) of the observed signal reveals that the oscillation is indeed periodic, featured by equally distributed spikes with very

narrow widths [see Fig. 4(c)]. The symmetry breaking process here also has a spontaneous feature: two repetitive realizations of the quench dynamics yield oscillations of the same pattern and periodicity, but can have completely different relative time phases. To quantify this characteristic, we extract the Fourier component $A(\omega_c)$ at the peak frequency ω_c for each experimental cycle, and plot it on the normalized complex plane [see Fig. 4(e)]. For 270 independent realizations, we identify a small fluctuation of the amplitude $|A(\omega_c)|$ (mainly limited by the resolution of the DFT) and a random distribution of its phase between 0 and 2π , which corroborates the spontaneous feature of the observed symmetry breaking order.

As a defining property, a CTC is predicted to be rigid, i.e., robust against temporal perturbations. To test the rigidity of the observed limit cycle, we add additional noises on the probe light with a bandwidth of 20 kHz [see Fig. 4(b)]. For a small but finite noise strength, we note that the ordered oscillation of the transmission signal will not suddenly disappear, but preserves its basic pattern in the noise-free case, also confirmed by a sharp peak of the Fourier spectrum at the same frequency [see Fig. 4(d)]. With increasing noise intensity, the oscillation pattern becomes much noisier, and we introduce a relative crystalline fraction Q to quantify such a melting process of the CTC, defined as $Q = \sum_{\omega \in \Delta\omega_c} A(\omega) / \sum_{\omega \in \Delta\omega} A(\omega)$, where $\Delta\omega_c$ is the width of oscillation fundamental frequency ω_c , and $\Delta\omega$ is the full spectral width. After normalized to the maximum crystalline fraction in the absence of added noise, we can obtain the relationship between noise intensity and relative crystalline fraction as shown in Fig. 4(f). As we can see, over a wide range of

noise parameters, the relative crystalline fraction can still maintain a comparatively large value, confirming that the observed dissipative time crystal is robust to temporal fluctuations of the continuous driving.

In summary, we experimentally demonstrate a dissipative time crystalline order in a room-temperature Rydberg atom ensemble, which is directly observed by the oscillatory transmission of probe beam. The oscillations originate from the simultaneous couplings to distinct Rydberg states, by which the competition between different Rydberg components facilitate the emergence of limit cycles. Importantly, the persistent oscillations spontaneously break the time translation symmetry and is robust against temporal perturbations, satisfying the defining properties of a CTC. Our work provides a realistic system for systematically investigating the dissipative time crystal, and also opens up a new route to quantum synchronization and sensing.

Note added. We recently became aware of two preprints on limit cycles in driven-dissipative systems.

In Ref. [41], a persistent auto-oscillation is observed in an electron-nuclear spin setup. In Ref. [42], a transient oscillation induced by Rydberg cluster is studied.

ACKNOWLEDGMENTS

We acknowledge valuable discussions with Klaus Mølmer, Yaofeng Chen, Yuanjiang Tang, Hadi Yarloo, and Huachen Zhang. This work is supported by the National Key R&D Program of China (Grant No. 2018YFA0306504 and No. 2018YFA0306503), the National Natural Science Foundation of China (NSFC) (Grant No. 92265205), and the Innovation Program for Quantum Science and Technology (2021ZD0302100). F. Yang and T. Pohl acknowledge the support from Carlsberg Foundation through the “Semper Ardens” Research Project QCool and from the Danish National Research Foundation (DNRF) through the Center of Excellence “CCQ” (Grant No. DNRF156).

[1] F. Wilczek, Phys. Rev. Lett. **109**, 160401 (2012).
[2] P. Bruno, Phys. Rev. Lett. **111**, 070402 (2013).
[3] H. Watanabe and M. Oshikawa, Phys. Rev. Lett. **114**, 251603 (2015).
[4] S. L. Sondhi, S. Girvin, J. Carini, and D. Shahar, Rev. Mod. Phys. **69**, 315 (1997).
[5] J. Eisert, M. Friesdorf, and C. Gogolin, Nat. Phys. **11**, 124 (2015).
[6] H. Haken, *Information and self-organization: A macroscopic approach to complex systems* (Springer Science & Business Media, 2006).
[7] F. Iemini, A. Russomanno, J. Keeling, M. Schirò, M. Dalmonte, and R. Fazio, Phys. Rev. Lett. **121**, 035301 (2018).
[8] H. Keßler, J. G. Cosme, M. Hemmerling, L. Mathey, and A. Hemmerich, Phys. Rev. A **99**, 053605 (2019).
[9] D. V. Else, B. Bauer, and C. Nayak, Phys. Rev. Lett. **117**, 090402 (2016).
[10] R. Khasseh, R. Fazio, S. Ruffo, and A. Russomanno, Phys. Rev. Lett. **123**, 184301 (2019).
[11] Z. Gong, R. Hamazaki, and M. Ueda, Phys. Rev. Lett. **120**, 040404 (2018).
[12] A. Lazarides, S. Roy, F. Piazza, and R. Moessner, Phys. Rev. Research **2**, 022002 (2020).
[13] A. Riera-Campeny, M. Moreno-Cardoner, and A. Sanpera, Quantum **4**, 270 (2020).
[14] A. Cabot, F. Carollo, and I. Lesanovsky, Phys. Rev. B **106**, 134311 (2022).
[15] R. J. L. Tuquero, J. Skulte, L. Mathey, and J. G. Cosme, Phys. Rev. A **105**, 043311 (2022).
[16] J. Zhang, P. W. Hess, A. Kyprianidis, P. Becker, A. Lee, J. Smith, G. Pagano, I.-D. Potirniche, A. C. Potter, A. Vishwanath, N. Yao, and C. Monroe, Nature **543**, 217 (2017).
[17] S. Choi, J. Choi, R. Landig, G. Kucska, H. Zhou, J. Isoya, F. Jelezko, S. Onoda, H. Sumiya, V. Khemani, C. Keeserlink, N. Yao, E. Demler, and M. Lukin, Nature **543**, 221 (2017).
[18] S. Pal, N. Nishad, T. Mahesh, and G. Sreejith, Phys. Rev. Lett. **120**, 180602 (2018).
[19] J. Rovny, R. L. Blum, and S. E. Barrett, Phys. Rev. Lett. **120**, 180603 (2018).
[20] A. Kyprianidis, F. Machado, W. Morong, P. Becker, K. S. Collins, D. V. Else, L. Feng, P. W. Hess, C. Nayak, G. Pagano, N. Yao, and C. Monroe, Science **372**, 1192 (2021).
[21] H. Taheri, A. B. Matsko, L. Maleki, and K. Sacha, Nat. Commun. **13**, 848 (2022).
[22] H. Keßler, P. Kongkhambut, C. Georges, L. Mathey, J. G. Cosme, and A. Hemmerich, Phys. Rev. Lett. **127**, 043602 (2021).
[23] X. Mi, M. Ippoliti, C. Quintana, *et al.*, Nature **601**, 531 (2022).
[24] J. Randall, C. Bradley, F. van der Gronden, A. Galicia, M. Abobeih, M. Markham, D. Twitchen, F. Machado, N. Yao, and T. Taminiau, Science **374**, 1474 (2021).
[25] J. G. Cosme, J. Skulte, and L. Mathey, Phys. Rev. A **100**, 053615 (2019).
[26] B. Buča, J. Tindall, and D. Jaksch, Nat. Commun. **10**, 1730 (2019).
[27] L. Bakker, M. Bahovadinov, D. Kurlov, V. Gritsev, A. K. Fedorov, and D. O. Krimer, Phys. Rev. Lett. **129**, 250401 (2022).
[28] D. Dreon, A. Baumgärtner, X. Li, S. Hertlein, T. Esslinger, and T. Donner, Nature **608**, 494 (2022).
[29] N. Dogra, M. Landini, K. Kroeger, L. Hruby, T. Donner, and T. Esslinger, Science **366**, 1496 (2019).
[30] M. Krishna, P. Solanki, M. Hajdušek, and S. Vinjanambath, Phys. Rev. Lett. **130**, 150401 (2023).
[31] T.-C. Guo and L. You, Frontiers in Physics **10** (2022).
[32] P. Kongkhambut, J. Skulte, L. Mathey, J. G. Cosme, A. Hemmerich, and H. Keßler, Science **377**, 670 (2022).
[33] T. E. Lee, H. Häffner, and M. Cross, Phys. Rev. A **84**, 031402 (2011).
[34] J. Qian, G. Dong, L. Zhou, and W. Zhang, Phys. Rev. A **85**, 065401 (2012).

- [35] C. Carr, R. Ritter, C. Wade, C. S. Adams, and K. J. Weatherill, Phys. Rev. Lett. **111**, 113901 (2013).
- [36] N. Šibalić, C. G. Wade, C. S. Adams, K. J. Weatherill, and T. Pohl, Phys. Rev. A **94**, 011401 (2016).
- [37] D.-S. Ding, H. Busche, B.-S. Shi, G.-C. Guo, and C. S. Adams, Phys. Rev. X **10**, 021023 (2020).
- [38] X. Wu, X. Liang, Y. Tian, F. Yang, C. Chen, Y.-C. Liu, M. K. Tey, and L. You, Chin. Phys. B **30**, 020305 (2021).
- [39] Y. He, Z. Bai, Y. Jiao, J. Zhao, and W. Li, Phys. Rev. A **106**, 063319 (2022).
- [40] H.-J. Su, J.-Y. Liou, I.-C. Lin, and Y.-H. Chen, Opt. Express **30**, 1499 (2022).
- [41] A. Greilich, N. Kopteva, A. Kamenskii, P. Sokolov, V. Korenev, and M. Bayer, arXiv:2303.15989 (2023).
- [42] D.-S. Ding, Z. Bai, Z.-K. Liu, B.-S. Shi, G.-C. Guo, W. Li, and C. S. Adams, arXiv:2305.07032 (2023).